

## The Diagnosis of Synoptic-Scale Vertical Motion in an Operational Environment

DALE R. DURRAN AND LEONARD W. SNELLMAN

*Department of Meteorology, University of Utah, Salt Lake City, UT 84112*

(Manuscript received 23 October 1985, in final form 22 December 1986)

### ABSTRACT

The physical reason for quasi-geostrophic vertical motion is reviewed. Various techniques for estimating synoptic-scale vertical motion are examined, and their utility (or lack thereof) is illustrated by a case study. The  $Q$ -vector approach appears to provide the best means of calculating vertical motions numerically. The vertical motion can be estimated by eye with reasonable accuracy by examining the advection of vorticity by the thermal wind or by examining the relative wind and the isobar field on an isentropic chart. The traditional form of the omega equation is not well suited for practical calculation.

### 1. Introduction

Every day the operational meteorologist is asked to absorb a tremendous amount of weather data and make a forecast. The National Meteorological Center makes this job easier by providing a number of products, such as MOS (Model Output Statistics) guidance, which can be used to formulate the forecast. However, "good" forecasters do not rely exclusively on computer generated guidance when making a forecast. They examine the developing weather patterns and attempt to understand the factors which are likely to be responsible for the current and next day's weather. Among the most important tools that the forecaster uses to analyze the future state of the atmosphere are the prognostic weather charts produced by numerical models such as the NGM (Nested-Grid Model) and LFM (Limited-Area Fine-Mesh Model).

One forecast variable which has a very pronounced effect on the weather is the vertical velocity. Sustained upward motion produces condensation and precipitation, destabilization of the lapse rate, and intensification of midlatitude cyclones. This important variable is represented by only one chart (the 700-mb vertical velocity) in the standard output format from the numerical models. In the same way that meteorologists do not accept the MOS guidance without examining the supporting evidence, they should also examine the factors which appear to be responsible for the vertical motion field. When they do this, they usually examine the vorticity advection and temperature advection patterns and connect the result with the quasi-geostrophic vertical velocity through the omega equation.

Barnes (1985) and Heflick and Fors (1979) have suggested that the quasi-geostrophic vertical velocity can be a useful forecasting tool. In order to use the quasi-geostrophic vertical velocity profitably, one needs to understand what it is and how to calculate it. Several

authors have previously considered the problem of diagnosing synoptic-scale vertical motion (Sutcliffe, 1947; Hoskins et al., 1978; Trenberth, 1978), and every modern dynamic meteorology textbook discusses quasi-geostrophic theory (Holton, 1979; Pedlosky, 1979); yet there still seems to be uncertainty among operational meteorologists about the physical significance of quasi-geostrophic motions and the methods by which they can be diagnosed. In this paper we will discuss the recent work of Hoskins et al. (1978) and Trenberth (1978) (hereafter referred to as HDD and TR, respectively) and demonstrate how their results can be applied in one case of practical interest.

### 2. What is the quasi-geostrophic vertical velocity?

Every meteorologist is aware that large-scale midlatitude motions are nearly in geostrophic and hydrostatic balance. Although the geostrophic and hydrostatic approximations provide a good description of the atmosphere at a given instant, the advections which are produced by a geostrophically balanced wind field act to destroy the thermal wind balance. When thermal wind balance is disrupted, the atmosphere must also be out of hydrostatic or geostrophic balance. Thus, in the absence of other effects, advection by the geostrophic wind will produce an atmospheric state which is very different from those actually observed. The effects of geostrophic advection are illustrated in the following example.

Consider the situation in Fig. 1, which shows the 500-mb height field, the 1000–500-mb thickness, and the 500-mb isotachs. The 1000-mb winds (not shown) are calm, in which case the 1000-mb height field is flat. Then, as shown in Fig. 1, the 1000–500-mb thickness lines must be parallel to the 500-mb height contours. Suppose that at the time shown, the flow is in perfect hydrostatic and geostrophic balance. Then the winds

are directed parallel to the temperature (thickness) field and there is no tendency for the geostrophic wind to change the temperature (thickness) pattern by advection. However, the winds are blowing across the isotachs from a region of high wind speed toward a region of low wind speed. In the absence of other factors, the geostrophic wind will advect itself in a manner which increases the wind speed throughout the entire region in Fig. 1. Since the temperature pattern has not changed, the tendency of the geostrophic wind to advect itself will disrupt either hydrostatic or geostrophic balance (or both). To be specific, suppose that the 500-mb heights remain consistent with the temperature (thickness) field, then the flow cannot remain in geostrophic balance because the wind speed will increase while the pressure gradient remains unchanged. On the other hand, if the 500-mb height field changes to geostrophically balance the changing wind field, the thickness field will not remain in hydrostatic balance with the temperature field.

The preceding is a specific example of the general result, proved in HDD, that geostrophic motion destroys itself by disrupting the thermal wind balance. Yet we know from practical experience that on the synoptic scale the atmosphere is never far from thermal wind balance (i.e., never far from hydrostatic and geostrophic balance). The balance is continually reestablished by ageostrophic circulations. The ageostrophic circulation which develops in the plane of cross section AB, Fig. 1, is shown in Fig. 2. The vertical motions increase the horizontal temperature gradient by adiabatic cooling in the north and adiabatic heating in the south. The horizontal ageostrophic motions decrease the vertical shear through the action of the Coriolis force. In this example, the northerly wind in the upper branch of the ageostrophic circulation decelerates the upper-level westerlies while the southerly wind on the lower branch accelerates the lower-level westerlies. Note how the changes due to these ageostrophic motions compensate for the tendency of the geostrophic motion to produce a vertical shear in the westerly wind

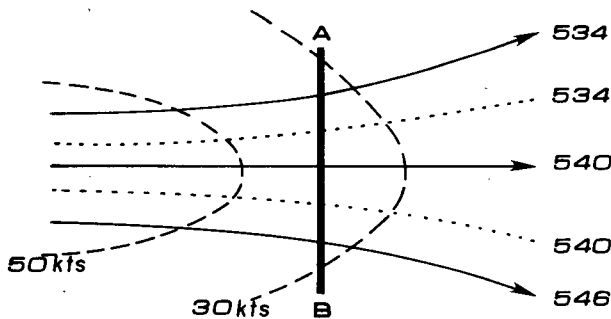


FIG. 1. 500-mb analysis for an idealized diffluent flow. Solid lines: 500-mb heights in dm; dotted lines: 1000-500-mb thickness in dm; dashed lines: 500-mb isotachs. Line segment AB indicates the location of the vertical cross section shown in Fig. 2.

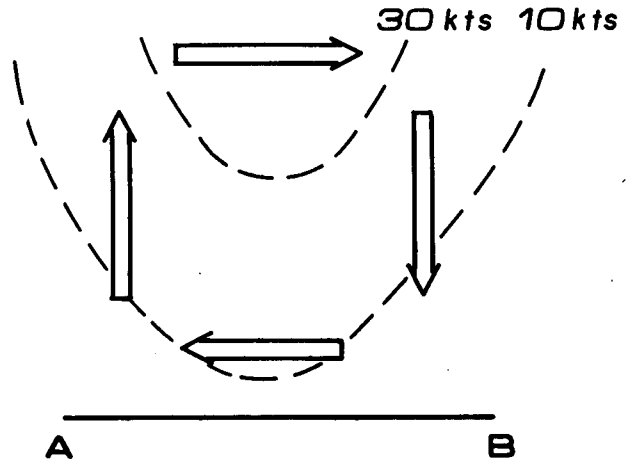


FIG. 2. Vertical cross section along line AB in Fig. 1. Dashed lines: isotachs; heavy arrows indicate the direction of the ageostrophic circulation.

which is too strong to be in thermal wind balance with the north-south temperature gradient.

The example in Fig. 1 is a special case in that the geostrophic wind does not change the thickness field by advection. The general case, where geostrophic advection is changing both the thickness and the wind field, is best analyzed in a frame of reference which moves with the geostrophic wind. Hoskins et al. (1978) have proved that when the changes produced by geostrophic advection in the thermal wind balance are observed in this frame of reference, the changes in the horizontal temperature-gradient term and the vertical shear term are equal in absolute value. However, the changes don't compensate because they have the wrong sign. Instead of compensating, the changes in the horizontal temperature gradient and the vertical wind shear contribute equally to the disruption of the thermal wind balance.

Most meteorologists can easily understand the physical processes which produce convection and orographic lifting. The preceding discussion has been presented in an attempt to clarify the processes which produce quasi-geostrophic vertical motion. The quasi-geostrophic vertical velocity (and ageostrophic horizontal winds) are those motions which are required to keep the geostrophic advection from producing large disruptions in the hydrostatic and geostrophic balances.<sup>1</sup> The quasi-geostrophic vertical velocity is valuable to the forecaster because the fundamental reason

<sup>1</sup> To be specific: The portion of the flow which is not in geostrophic balance is constrained to be a factor on the order of the Rossby number, weaker than the portion which is in geostrophic balance. The Rossby number is defined as  $U/fL$  where  $U$  is a characteristic velocity,  $L$  a characteristic length scale and  $f$  is the Coriolis parameter. The Rossby number associated with synoptic scale, midlatitude motion is approximately 1/10.

for its existence can be easily understood, it can be calculated without unreasonable difficulty, and it is a good approximation to the total vertical velocity in synoptic scale systems.

### 3. Determining the quasi-geostrophic vertical velocity

The vertical velocity required to maintain thermal wind balance is generally computed from the quasi-geostrophic omega equation:

$$\underbrace{\left(\sigma \nabla^2 + f_0^2 \frac{\partial^2}{\partial p^2}\right) \omega}_{\substack{\text{3D "Laplacian" \\ of omega}}} = \underbrace{f_0 \frac{\partial}{\partial p} \left[ \mathbf{V}_g \cdot \nabla \left( \frac{1}{f_0} \nabla^2 \Phi + f \right) \right]}_{\substack{\text{increase with height in} \\ \text{the vorticity advection}}} + \underbrace{\nabla^2 \left[ \mathbf{V}_g \cdot \nabla \left( \frac{-\partial \Phi}{\partial p} \right) \right]}_{\substack{\text{2D Laplacian of} \\ \text{the temperature} \\ \text{advection}}} \quad (1)$$

where the significance of each term is denoted in English, and the notation follows Holton (1979). This form can be used for numerical calculation (Haltiner, 1971), but unfortunately, most operational meteorologists do not have access to systems programmed to perform this calculation in real time. As a consequence, the meteorologist who wishes to examine the synoptic-scale vertical motion field must attempt to solve Eq. (1) in his head. This is not easy, and a number of approximations must be made.

One very common approximation is to assume that the left-hand side of (1) is proportional to  $-\omega$ . This allows the vertical velocity to be estimated from the forcing terms on the right-hand side of (1) without performing the complex numerical calculations required to invert a three-dimensional differential operator. We make this approximation throughout the remainder of this paper, although it does introduce error. The nature of the error, which is examined in detail in appendix A, is twofold. First, the spatial variation in  $\omega$  is smoother than that of the right-hand side forcing because the integration of (1) tends to damp the short wavelengths. Second, the vertical coupling, introduced by the second derivative with respect to pressure on the left-hand side of (1), tends to make this approximation most accurate in the middle troposphere where  $\omega$  is least influenced by the forcing at other levels.

The following sections of this paper discuss the various approximations which have been used to evaluate the right-hand side of (1), and illustrate their usefulness (or lack thereof) in diagnosing vertical motion patterns and precipitation over the northwestern United States on 12 February 1986. The synoptic situation at 1200 UTC 12 February 1986 is shown by the 850-, 700-, 500- and 300-mb analyses in Fig. 3. Each height field

in Fig. 3 was derived from a hand analysis of the original sounding data. The hand analyses were subsequently digitized onto a  $1^\circ$  latitude by  $1^\circ$  longitude grid. Short-wavelength noise was removed from the digitized data with a fourth-order smoother. The smoothed data were objectively contoured to produce Fig. 3 and were used for all calculations described in the following sections. The 1200 UTC surface map is shown in Fig. 4. Note the large area of precipitation running from southwest Oregon to eastern Washington. A separate band of precipitation is apparent along the coast in northern California, which appears to be related to an approaching warm front.

### 4. The standard form of the omega equation

The second term on the right-hand side of (1) is often assumed to be proportional to  $-1$  times the temperature advection. Although this assumption can be rigorously justified when the disturbance has the structure of a single sinusoidal wave (Holton, 1979), it may not hold in more complex situations where the disturbance is the sum of several waves of different wavelengths.

The shortcomings of this approximation are illustrated in Fig. 5a, which shows the 700-mb heights and the 850-500-mb thickness fields for our sample case. A large region of warm advection is present, centered over eastern Oregon. The exact extent of the warm advection is displayed in Fig. 5b which shows contours of  $-1$  times the strength of the temperature advection. (The temperature advection,  $\mathbf{V}_g \cdot \nabla(-\partial\Phi/\partial p)$  is negative for warm advection, so scaling the plot in Fig. 5b by  $-1$  ensures that positive areas correspond to warm advection.) If, as just discussed, the Laplacian of the temperature advection is assumed to be proportional to  $-1$  times the advection itself, the positive areas in Fig. 5b should also be areas where the second term in (1) is forcing upward motion. In fact, as illustrated in Fig. 5c, the actual area in which the Laplacian of the temperature advection is positive is much smaller. Note the region along the Oregon-Nevada border where there is strong warm advection, but the Laplacian of the warm advection is negative; this area, where warm advection is associated with downward motion, is shaded in Fig. 5a.

It is not uncommon to estimate the first term in (1) from the vorticity advection at a single level (usually the 500-mb level). This approximation can also lead to error, as illustrated in Fig. 6. Figure 6a shows the 500-mb height and vorticity fields, and indicates strong positive vorticity advection (PVA) in northwestern Oregon, with a region of negative vorticity advection (NVA) farther east. The contours of 500-mb vorticity advection (times  $-1$ ) shown in Fig. 6b may be compared with the increase in vorticity advection with height plotted in Fig. 6c. The increase in vorticity advection with height forces vertical motions which are

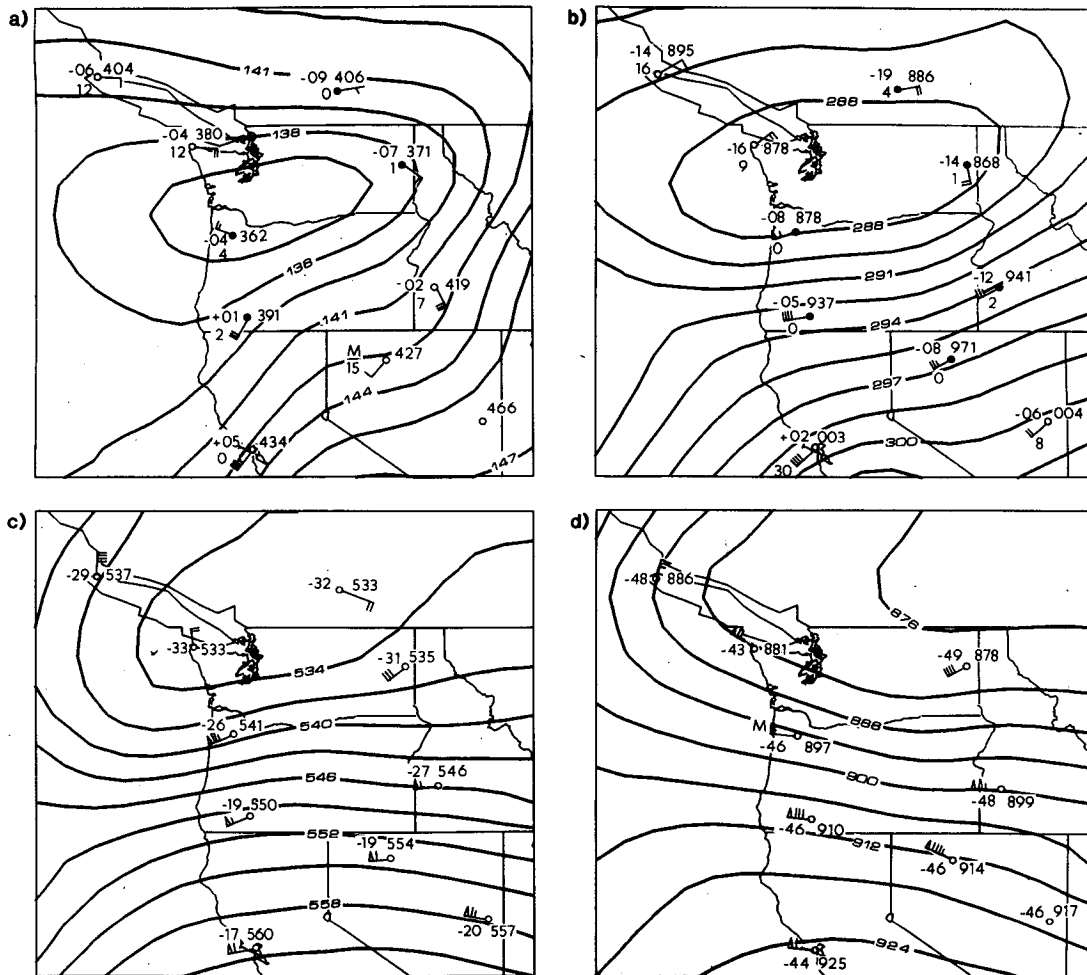


FIG. 3. Contours of the gridded data for 1200 UTC 12 February 1986. (a) 850 mb, 15-dm contour interval; (b) 700 mb, 15-dm contour interval; (c) 500 mb, 30-dm contour interval; (d) 300 mb, 60-dm contour interval.

rather different from those suggested by the 500-mb vorticity advection; note the region in northeastern Oregon where there is NVA at 500 mb, but the change in vorticity advection with height favors upward motion.

The results shown in Figs. 5 and 6 may be discouraging in that they suggest that a careful evaluation of the forcing terms in the omega equation can be a rather laborious process. The true situation is actually worse since the total forcing for the vertical velocity is the sum of the two individual terms, and in the general case where both terms are nonzero, they often oppose. The complexity of the final result is illustrated in Figs. 7 and 8. Figure 7a shows the contribution to the forcing from the increase in vorticity advection with height at 700 mb, and Fig. 7b shows the total 700-mb forcing, which is the sum of the fields in Fig. 5c and Fig. 7a. Figure 8a shows the forcing due to the Laplacian of the warm advection at 500 mb, and Fig. 8b shows the total 500-mb forcing (sum of Figs. 6c and 8a). At both 700 and 500 mb, there is considerable difference between the individual forcing terms and their total, sug-

gesting that the final result can hardly be estimated without recourse to numerical computation.

### 5. Trenberth's approximation

How can the quasi-geostrophic vertical velocity be estimated best by a forecaster without access to a computer? Trenberth (1978) has shown that the mathematical forcing terms in the omega equation may be expressed as

Increase in vorticity advection with height

$$= \text{advection of absolute vorticity by the thermal wind} \\ + \text{advection of thermal vorticity by the wind} \quad (2a)$$

Laplacian of warm advection

$$= \text{advection of relative vorticity by the thermal wind} \\ - \text{advection of thermal vorticity by the wind} \\ + \text{terms involving the deformation of the wind field} \quad (2b)$$

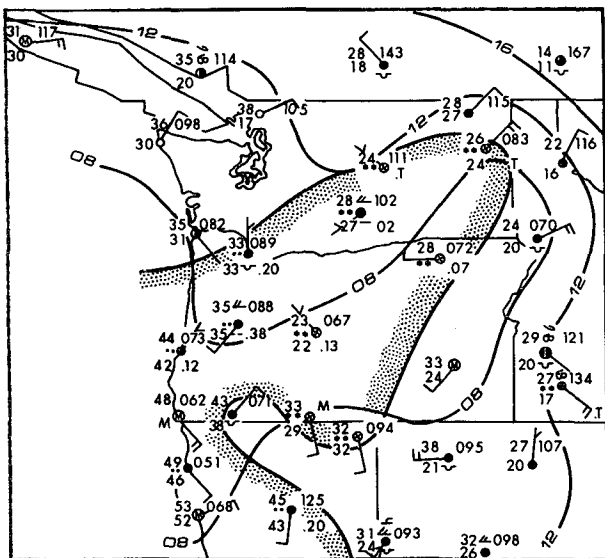


FIG. 4. Surface analysis for 1200 UTC 12 February 1986. Area of active precipitation is shaded. The break in the precipitation between Oregon and California is supported by the Medford observation and satellite photos.

(where absolute vorticity is the relative vorticity of the wind plus the earth's vorticity,  $f$ ). Note that the term involving the advection of thermal vorticity by the wind cancels between the two expressions. As discussed in TR, one can ignore the difference between the advection of relative and absolute vorticity and approximate the omega equation with minimal loss of accuracy as

$$\underbrace{\left(\sigma \nabla^2 + f_0 \frac{\partial^2}{\partial p^2}\right) \omega}_{\text{advection of vorticity by the thermal wind}} = 2f_0 \frac{\partial \mathbf{V}_g}{\partial p} \cdot \nabla \left( \frac{1}{f_0} \nabla^2 \Phi \right) + \left( \text{terms involving the deformation of the wind field} \right). \quad (3)$$

As demonstrated in TR, in the middle troposphere, the right-hand side of (3) is dominated by the contribution from the advection of vorticity by the thermal wind. Thus synoptic-scale ascent should occur in regions where there is advection of cyclonic vorticity by the thermal wind. This criteria is equivalent to that obtained by Sutcliffe (1947). Trenberth's approach has the advantage that it can be used on AFOS (Automation of Field Operations and Services) facilities without special programming by superimposing the 500-mb vorticity and 1000-500-mb thickness fields. Figure 9 shows the forcing for the quasi-geostrophic vertical velocity at 700 and 500 mb as diagnosed from (3) (ignoring the deformation terms). It may be seen that this approach gives a reasonably good approximation to the total forcing (compare with Fig. 11).

### 6. Hoskins' approach

If a forecaster must estimate the vertical velocity without the aid of special computer programs, he will probably get the best result (and certainly get it with the least effort) by using the Trenberth-Sutcliffe approximation. However, as computers become progressively more powerful and less expensive, it is likely that most forecasters will have access to them, and in that case, they will be able to compute the total quasi-geostrophic vertical velocity using a numerical scheme which solves the complete omega equation.

When evaluating the vertical velocity numerically, the forecaster will also have the opportunity to examine the relative strength of each of the forcing terms in (1). However, such efforts are likely to be a waste of time. Hoskins et al. (1978) have stressed that the advection of thermal vorticity [which cancels between the two forcing terms in (2)] will change as the mean wind speed changes. Thus, if we attempt to calculate the vertical velocities in two identical weather systems embedded in uniform mean flows moving at two different speeds, the individual forcing terms in (1) will be different in the two cases. On the other hand, the actual vertical motion field, and the fundamental mechanisms which produce it, will be the same, suggesting that the individual terms on the right-hand side of (1) do not have intrinsic physical significance. Neither the Laplacian of the warm advection nor the rate of change of vorticity advection with height should be regarded as a cause of synoptic-scale vertical motion. As discussed in section 2, quasi-geostrophic vertical motion is "caused" by the tendency for advection by the geostrophic wind to destroy thermal wind balance.<sup>2</sup>

What, if anything, might the forecaster ask the computer to display besides the total forcing? The answer suggested by HDD is  $Q$ -vectors, defined as

$$\mathbf{Q} = \left[ \frac{\partial \mathbf{V}_g}{\partial x} \cdot \nabla \left( \frac{\partial \Phi}{\partial p} \right), \frac{\partial \mathbf{V}_g}{\partial y} \cdot \nabla \left( \frac{\partial \Phi}{\partial p} \right) \right]. \quad (4)$$

The  $Q$ -vector is equal to the rate of change of the horizontal potential temperature gradient, which would develop in a fluid parcel moving with the geostrophic wind if the vertical velocity was exactly zero.<sup>3</sup> An alternate interpretation of the  $Q$ -vector (Hoskins and

<sup>2</sup> The ultimate cause of synoptic scale vertical motion might be best attributed to solar heating, which drives the general circulation.

<sup>3</sup> However, at the level of the quasi-geostrophic approximation, the vertical velocity is not zero and

$$\mathbf{Q} = \frac{D_g}{Dt} \nabla_h \theta + \frac{\theta_0}{g} N^2 (\nabla_h w),$$

in which case the "frontogenesis function" (the change in magnitude of the horizontal temperature gradient following a parcel moving with the geostrophic wind) is

$$\frac{D_g}{Dt} |\nabla_h \theta|^2 = 2 \nabla_h \theta \cdot \mathbf{Q} - 2 N^2 \frac{\theta_0}{g} \nabla_h \theta \cdot \nabla_h w,$$

where the notation follows Hoskins and Pedder (1980).

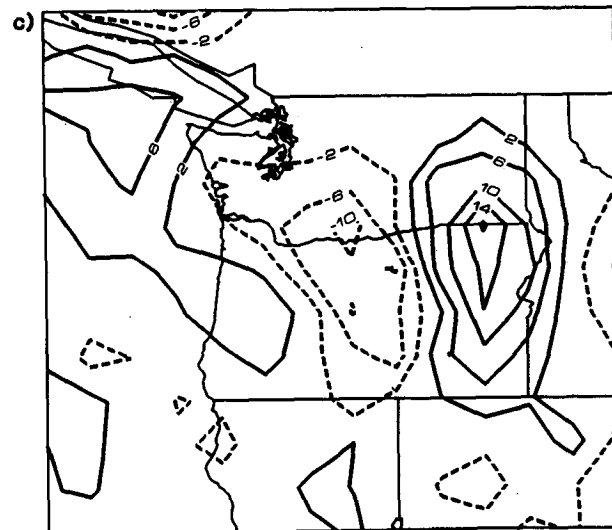
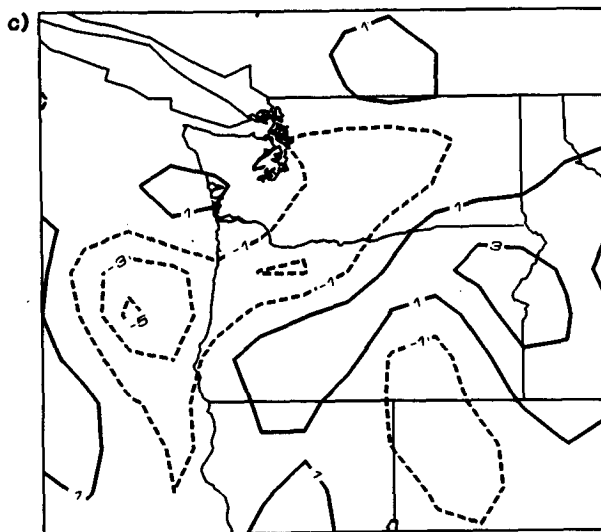
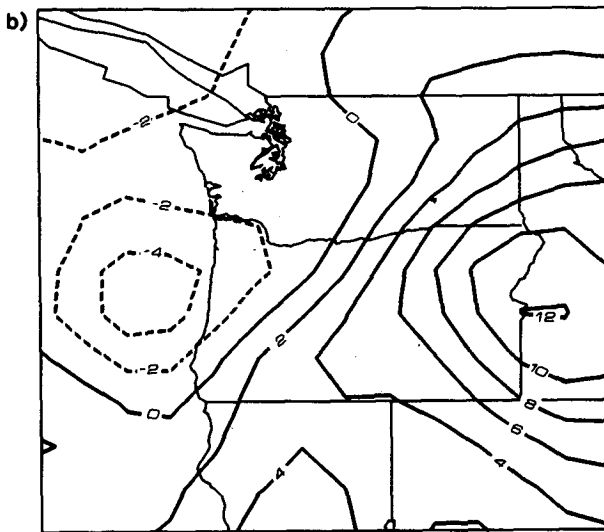
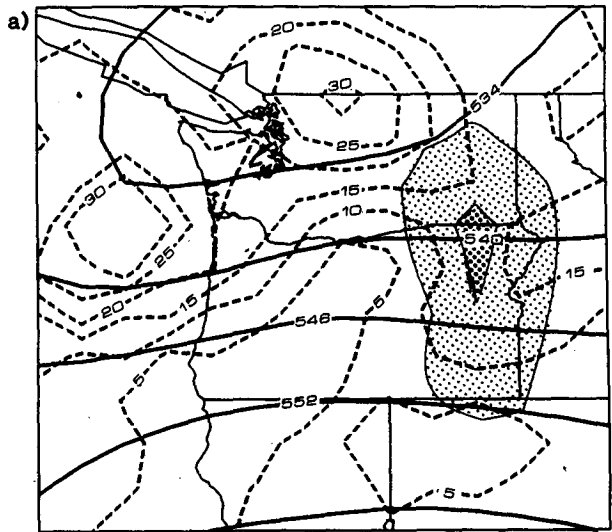
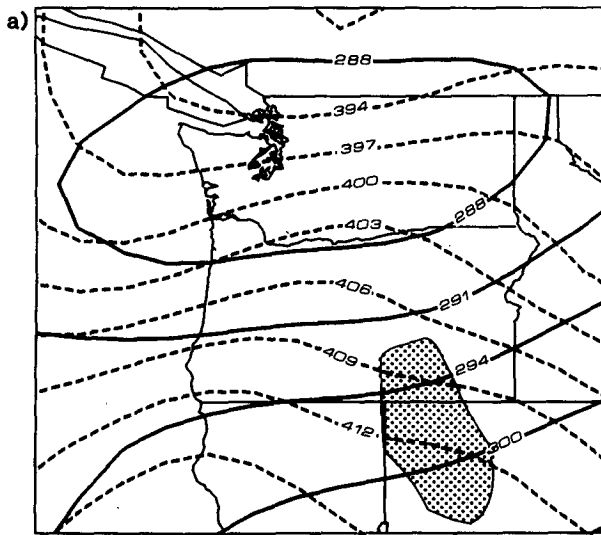


FIG. 5. (a) 700-mb heights (solid) and 850-500-mb thickness (dashed); shading shows an area where Laplacian of warm advection forces downward motion. (b)  $-1$  times 700-mb warm advection; contour interval  $2 \times 10^{-7} \text{ m}^3 \text{ kg}^{-1} \text{ s}^{-1}$ . (c) Laplacian of the 700-mb warm advection; contour interval  $2 \times 10^{-17} \text{ m} \text{ kg}^{-1} \text{ s}^{-1}$ .

FIG. 6. (a) 500-mb heights (solid) and absolute vorticity (dashed); shading shows area where increase in vorticity with height forces upward motion; strongest forcing is indicated by dark shading. (b) 500-mb vorticity advection, contour interval  $4 \times 10^{-9} \text{ s}^{-2}$ . (c) increase in vorticity advection with height at 500 mb, contour interval  $4 \times 10^{-17} \text{ m} \text{ kg}^{-1} \text{ s}^{-1}$ .

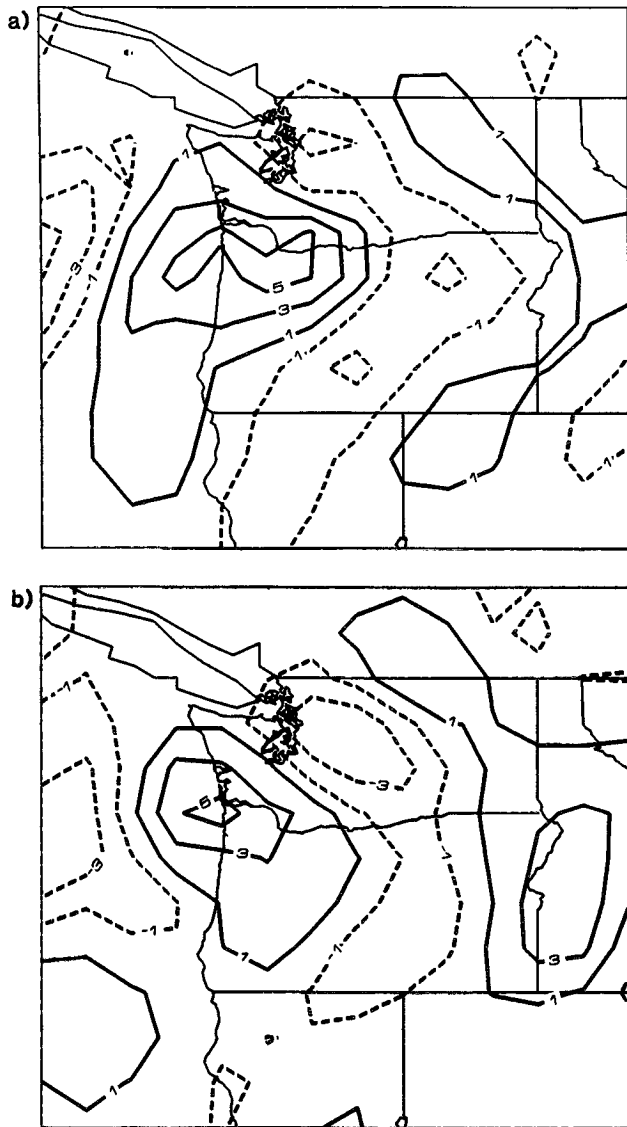


FIG. 7. (a) Increase in vorticity with height at 700 mb. (b) Total forcing for  $\omega$  at 700 mb. Contour interval is  $2 \times 10^{-17} \text{ m kg}^{-1} \text{ s}^{-1}$  in both plots.

Pedder, 1980) is that it provides an approximate picture of the ageostrophic horizontal wind in the lower branch of the circulation that develops in order to maintain thermal wind balance in an evolving synoptic disturbance (see Fig. 2). It points toward the rising motion, and its magnitude is roughly proportional to the strength of the ageostrophic horizontal wind. The 500-mb  $Q$ -vector field at 1200 UTC 12 February 1986 is plotted in Fig. 10, which shows that the rising motions producing the precipitation in northwestern Oregon are part of an ageostrophic circulation with strong, low-level flow into the region from the northwest.

As shown by HDD, the right-hand side of (1) is exactly equivalent to  $-2$  times the divergence of  $Q$ , i.e.,

the forcing for quasi-geostrophic vertical motion may be diagnosed from the divergence of  $Q$ . The divergence of the  $Q$ -vectors (times  $-2$ ) is plotted in Fig. 11. Although Fig. 11 is in general agreement with the result in Figs. 7b and 8b, the details differ considerably. These differences are due to the fact that the finite difference forms for the divergence of the  $Q$ -vectors and the right-hand side of (1) are not identical. (The finite difference expressions are given in appendix B.) As discussed earlier, there is a large term, the advection of thermal vorticity by the wind, which cancels between the increase in vorticity advection with height and the Laplacian of the warm advection in the conventional form of the

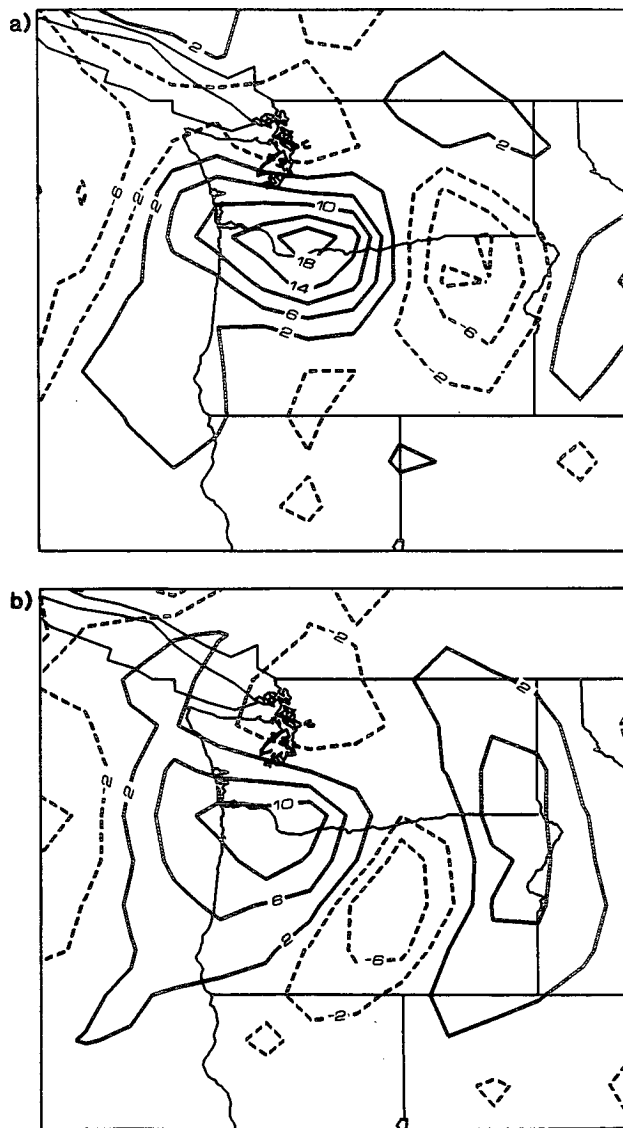
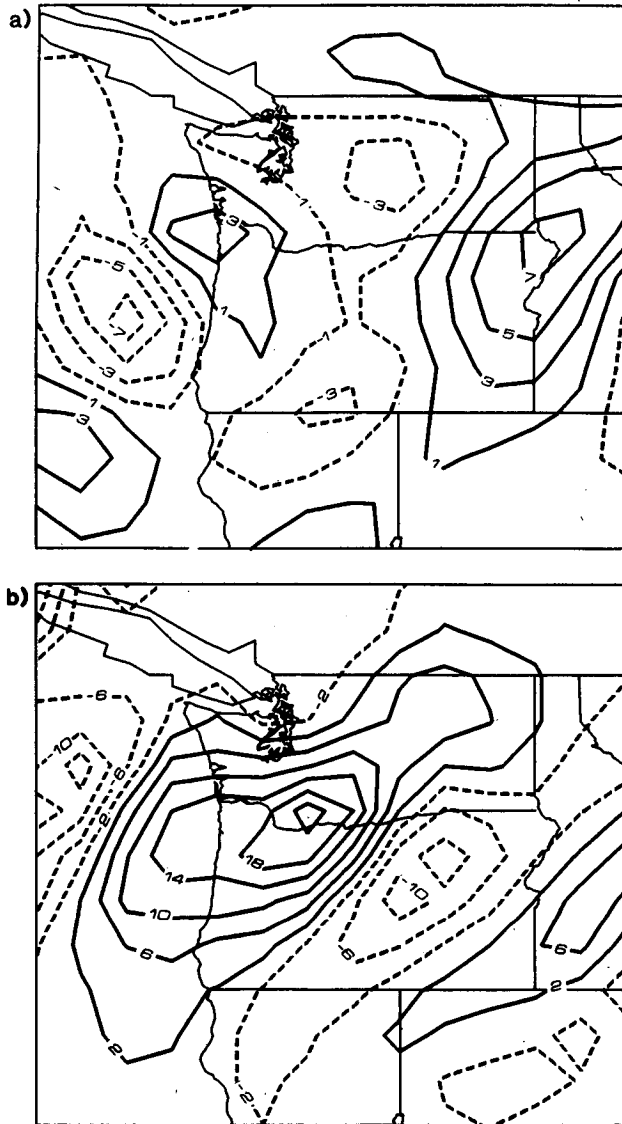


FIG. 8. (a) Laplacian of 500-mb warm advection. (b) Total forcing for  $\omega$  at 500 mb. Contour interval is  $4 \times 10^{-17} \text{ m kg}^{-1} \text{ s}^{-1}$  in both plots.



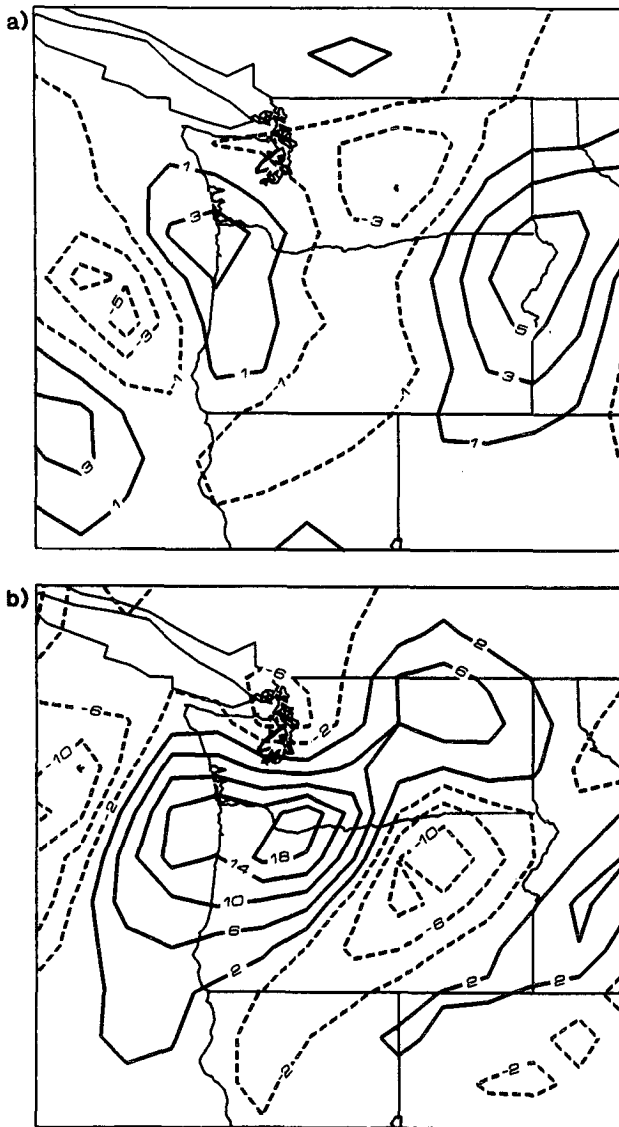


FIG. 11. Divergence of the  $Q$ -vectors (times  $-2$ ) at (a) 700 mb; contour interval  $2 \times 10^{-17} \text{ m kg}^{-1} \text{ s}^{-1}$ . (b) 500 mb; contour interval  $4 \times 10^{-17} \text{ m kg}^{-1} \text{ s}^{-1}$ .

### 7. Utility of the quasi-geostrophic vertical velocity

A comparison of Fig. 11b with the areas of active precipitation reported on the surface map (Fig. 4) shows that the 500-mb forcing for  $\omega$  provides a good diagnosis of the primary rain area which extends from southwestern Oregon to northwestern Washington. However, there is no forcing for upward motion associated with the precipitation along the California coast. It is possible that the precipitation in California is associated with orographic or mesoscale phenomena which would not be revealed by our quasi-geostrophic calculations; it is also possible that the lack of diagnosed upward motion is due to deficiencies in the analysis of the flow in the data-poor area over the eastern Pacific. Northern

California notwithstanding, the overall agreement between the calculations in Fig. 11b and the observations in Fig. 4 is very good, suggesting that quasi-geostrophic diagnostics can be a valuable aid in precipitation forecasting.

At 500 mb, the sum of the increase in vorticity advection with height and the Laplacian of the warm advection (Fig. 8b) do not correlate with the observed precipitation pattern as well as the divergence of the 500-mb  $Q$ -vectors (Fig. 11b). In this particular case, it appears that the increased accuracy in the  $Q$ -vector calculations leads to an improved diagnosis of the vertical motion field.

The correlation between the forcing at 700 mb and the observed precipitation is not nearly as good. As this might suggest, the 700-mb  $Q$ -vector divergence is rather different from the  $Q$ -vector divergence at 500 mb. Note, however, that there is considerably more vertical consistency in the conventional forcing calculations (Figs. 7b, 8b) than in the more accurate  $Q$ -vector calculations (Figs. 11a, b). Barnes and Gyakum (personal communications) have suggested that although there is generally a good correlation between the 700- and 500-mb  $Q$ -vector divergence, cases with poor vertical consistency are not uncommon. The relatively poor agreement between the 700- and 500-mb  $Q$ -vector divergence shown in Figs. 14 and 16 of Barnes (1985) is similar to that encountered in this case study.

It is important to appreciate that a poor correlation between the  $Q$ -vector divergence does not imply a poor correlation between the 700- and 500-mb  $\omega$ . As discussed in appendix A, the vertical derivative term on the left-hand side of (1), together with the top and bottom boundary conditions, constrain the 700-mb  $\omega$  to be relatively insensitive to the 700-mb forcing when the horizontal length scale of the disturbance is larger than 1000 km. Under these circumstances it is possible that the 700-mb vertical motion will be more reliably diagnosed from the 500-mb  $Q$ -vector divergence than from the 700-mb  $Q$ -vector divergence. This reasoning is in agreement with the findings in TR that the actual omega, obtained after inverting the differential operator on the left-hand side of the omega equation, most closely corresponds to the right-hand side forcing in the midtroposphere (600–400 mb).

### 8. The thermodynamic method

There are alternate methods for diagnosing synoptic-scale vertical motions which do not rely on the omega equation. One of the most popular of these is the thermodynamic method, which is used to diagnose vertical motions on isentropic charts. The vertical motion at a point on an isentropic chart is proportional to the wind speed relative to the motion of the isentropic surface times the isentropic pressure-gradient in the direction of the relative wind vector (Saucier, 1955). Note that the velocity which matters is the relative wind, so that

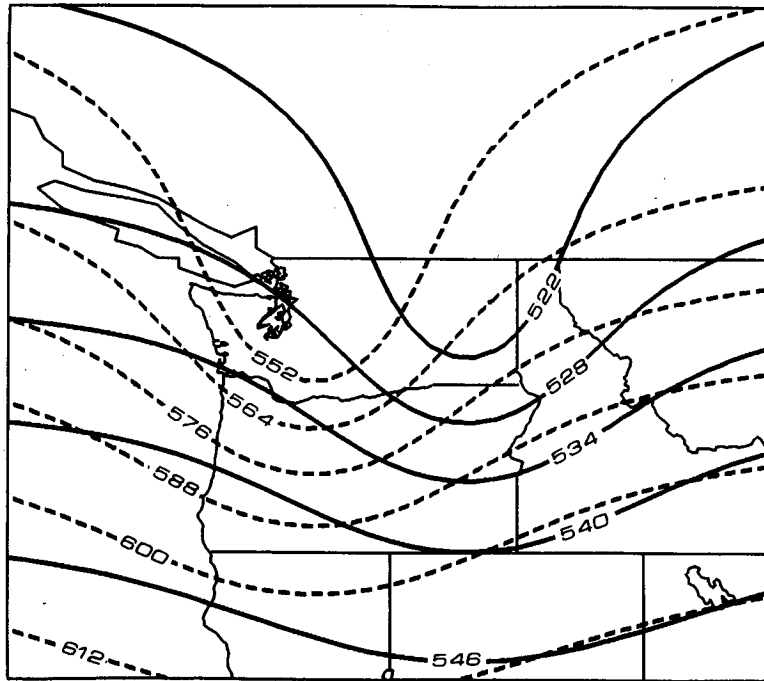


FIG. 12. Contours of 500-mb height (solid) and 700–300 mb thickness (dashed) for the height field specified analytically in appendix C.

the vertical motion is a function of the difference between the local rate of change of the potential temperature and the horizontal temperature advection. No information can be obtained by considering either term individually. This problem is the same one which clouds the meaning of the individual terms on the right-hand side of the conventional omega equation; their values change if there are changes in the mean speed of the flow in which the system is imbedded.

An isentropic chart for the  $\theta = 294$  K surface is shown in Fig. 14. The isentropic chart is the result of a hand analysis; it was not computed directly from the gridded data. Figure 14 shows a broad region of warm advection in central and eastern Oregon where strong winds are directed sharply across the isobars toward lower pressure. A rough indication of the motion of the  $\theta$ -surface can be obtained from the dotted line in Fig. 14, which shows the numerically forecast position of the 700-mb isobar on the same 294 K surface 12 h later. Note that the  $\theta$ -surface moves rapidly downwind in southeastern Oregon, but it moves very little in the northwest. Thus the strongest upward motion actually occurs in western Oregon, where the relative wind component across the isobars is greatest.

In summary, the thermodynamic method appears to give results which are consistent with the observed precipitation pattern and the results obtained earlier from the omega equation. In fact, since the omega equation is derived solely from the quasi-geostrophic vorticity and thermodynamic equations, our results

must agree (provided the flow can be adequately described by the quasi-geostrophic approximation). It is difficult to make a more quantitative comparison because the instantaneous rate at which the  $\theta$ -surface is moving cannot be accurately estimated from the 12-h rawinsonde reports. This problem with quantitative accuracy is the reason that meteorologists generally use the omega equation, which does not require the evaluation of time derivatives, for numerical computation of the vertical velocity. However, isentropic charts provide a very useful way of visualizing the three-dimensional airflow and obtaining a rough estimate of the vertical velocity.

## 9. Conclusions

We have reviewed the nature of quasi-geostrophic vertical motion, emphasizing the physical picture that this motion develops in order to maintain the hydrostatic and geostrophic balance which would otherwise be destroyed by the advective effects of the geostrophic wind. We have examined the airflow over the Pacific Northwest on 12 February 1986 and found that there is good agreement between the observed precipitation pattern and the quasi-geostrophic vertical motion as diagnosed from the 500-mb forcing terms in the omega equation. We have applied several commonly used approximations and techniques for the calculation of synoptic-scale vertical motion to this case in order to illustrate the accuracy and utility of each method.

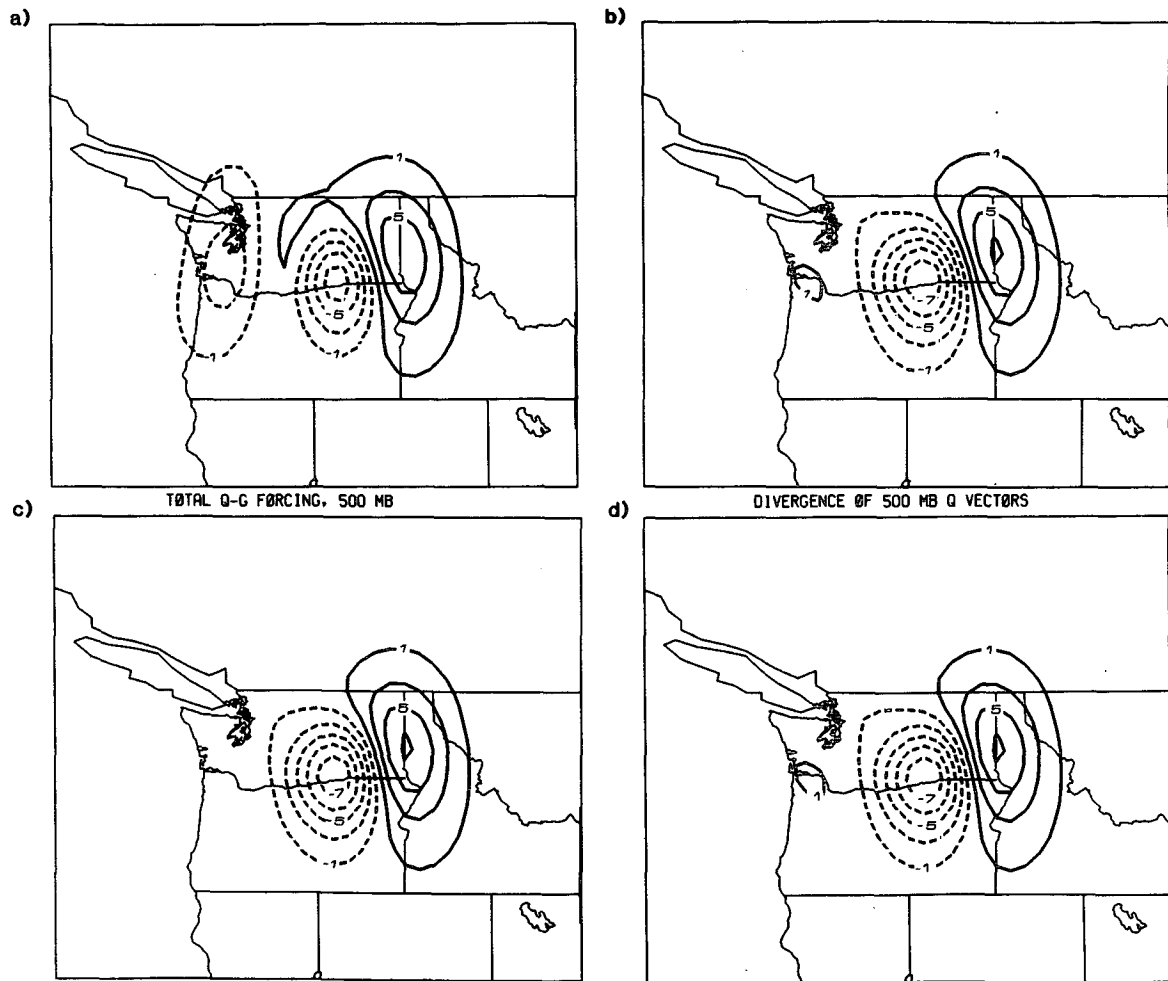


FIG. 13. Total forcing for  $\omega$ . (a)  $\Delta p = 200$  mb: conventional calculation, (b)  $\Delta p = 200$  mb: divergence of  $Q$ -vectors, (c)  $\Delta p = 50$  mb: conventional calculation, (d)  $\Delta p = 50$  mb: divergence of  $Q$ -vectors. Contour interval is  $2 \times 10^{-16} \text{ m kg}^{-1} \text{ s}^{-1}$ .

As is common practice, we did not actually solve the omega equation for  $\omega$ . Instead we assumed that the differential operator acting on  $\omega$  produces a result which is proportional to  $-\omega$ . According to this approximation, the vertical velocity can be determined from the strength and sign of the "forcing" terms in the omega equation without having to solve a three-dimensional partial differential equation. Trenberth (1978) has suggested that this approximation works best in the mid-troposphere. This is consistent with our finding that the vertical motions diagnosed from the 500-mb forcing agreed with the observed precipitation better than those diagnosed from the 700-mb forcing. As discussed in appendix A, it appears that the vertical coupling, introduced through the vertical derivative in the operator acting on  $\omega$ , reduces the sensitivity of the 700-mb  $\omega$  to the 700-mb forcing. When the horizontal length scale of a disturbance exceeds 1000 km, the vertical coupling may be significant and, in cases such as ours, the

700-mb forcing may be poorly correlated with the 700-mb  $\omega$ .

In the traditional form of the omega equation, the forcing terms are the increase in vorticity advection with height and the Laplacian of the warm advection. We have cited examples from this case study which demonstrate that the increase in vorticity advection with height cannot be reliably estimated from the vorticity advection at a single level and that the warm advection itself cannot be used as a substitute for the Laplacian of the warm advection. In particular, we exhibited regions in which there was NVA, but the increase in vorticity advection with height forced upward motion, and regions in which there was warm advection, but the Laplacian of the warm advection forced downward motion.

It is thus rather difficult to estimate either of the individual forcing terms in the traditional form of the omega equation. As a consequence, it is all but im-

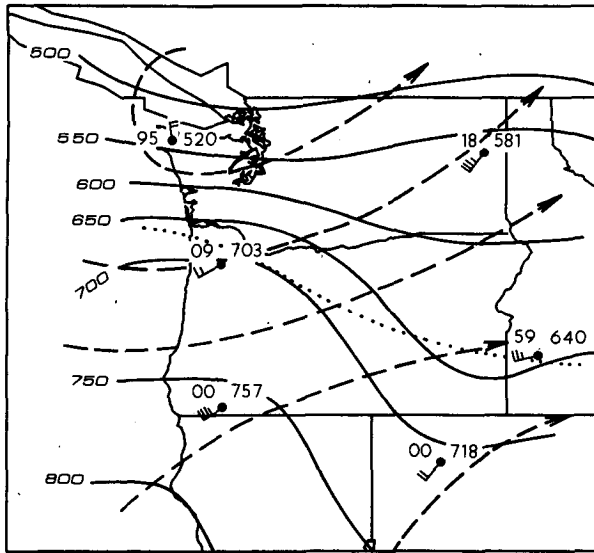


FIG. 14. Isentropic chart for the 294 K surface at 12Z on 12 February 1986. Pressure is plotted to the right of the station, condensation pressure depression is plotted on the left. Isobars are solid lines, streamlines are dashed. The dotted line gives the position of the 700-mb isobar on the same 294 K surface 12 h later, at 0000 UTC 13 February.

possible to estimate their sum, the total forcing, without numerical calculation. If one is trying to formulate a mental estimate of the synoptic scale vertical motion, the easiest and most accurate approach is to examine the advection of vorticity by the thermal wind as suggested by Trenberth (1978) and Sutcliffe (1947). This can be done on the AFOS system by superimposing the 500-mb vorticity and the 1000–500-mb thickness field. As an alternative approach, one could examine the isobars and relative winds on an isentropic chart.

If one is computing the forcing terms in the omega equation numerically, it is best to compute the divergence of the  $Q$ -vectors (Hoskins et al., 1978). One advantage of the  $Q$ -vector approach is that the vectors themselves have physical significance, providing a visualization of the low-level branch of the ageostrophic circulation which supports the vertical motion (Hoskins and Pedder, 1980). Another significant advantage is that the computation of the divergence of the  $Q$ -vectors is subject to less numerical error. A large term, the advection of thermal vorticity by the wind, cancels between the two forcing terms in the traditional form of the omega equation. In cases where the numerical resolution is poor, the cancellation will not be exact and the residual may produce a significant error. The  $Q$ -vector approach does not suffer from this difficulty, and neither does the approximate form suggested by Trenberth (1978) and Sutcliffe (1947). It is interesting to note that in this case study, the advection of vorticity by the thermal wind is in better agreement with the divergence of the  $Q$ -vectors and the observed precipitation pattern than is the finite difference form of the traditional forcing terms.

*Acknowledgments.* Peter Miller assisted with the digitization of the dataset. This research was supported by NSF Grant ATM-8320695. The manuscript benefited from comments made by two anonymous reviewers.

#### APPENDIX A

##### Difference Between $\omega$ and the Right-Hand Side Forcing

The approximation that  $\omega$  is proportional to  $-1$  times the right-hand side forcing ( $F_{RHS}$ ) is exact if the spatial variation in  $F_{RHS}$  is sinusoidal and confined to a single coordinate and wavelength, i.e., if

$$F_{RHS} = \sin kx \quad (A1)$$

(1) reduces to

$$\sigma \frac{d^2 \omega}{dx^2} = \sin kx \quad (A2)$$

which has the solution

$$\omega = -\frac{1}{k^2 \sigma} \sin kx. \quad (A3)$$

Clearly in this case  $\omega$  is proportional to  $-1$  times  $F_{RHS}$ . Now consider the case where  $F_{RHS}$  is the sum of forcing at two different wavelengths:

$$F_{RHS} = \sin kx + \sin 2kx. \quad (A4)$$

In this case the solution to (1) becomes

$$\omega = -\frac{1}{k^2 \sigma} \left( \sin kx + \frac{1}{4} \sin 2kx \right) \quad (A5)$$

and  $\omega$  is no longer proportional to  $-1$  times  $F_{RHS}$ . The short wavelength ( $\sin 2kx$ ) and long wavelength ( $\sin kx$ ) terms contribute equally to  $F_{RHS}$ , but the contribution to  $\omega$  from the short wavelength term is a factor of 4 less than that from the long wavelength term. Therefore, since the amplitude of short-wavelength features is reduced when the left-hand side of (1) is integrated, a contour plot of  $\omega$  should appear to be smoother than a horizontal contour plot of the right-hand side forcing.

A potentially more serious error is introduced through the vertical second derivative in the left-hand side of (1) which couples the  $\omega$  at a given point to the right-hand side forcing throughout an entire column of the troposphere. Let us temporarily assume that the vertical second derivative term dominates the horizontal Laplacian terms on the left-hand side of (1), in which case the omega equation may be written:

$$f_0^2 \frac{d^2 \omega}{dp^2} = F_{RHS}. \quad (A6)$$

The average vertical velocity profile calculated in the central portion of an extratropical cyclone (Palmen and Newton, 1969, p. 383) is plotted as a dashed line in Fig. A1. In the following we determine values for  $F_{RHS}$  at 500 and 700 mb which allow the solution of (A6)

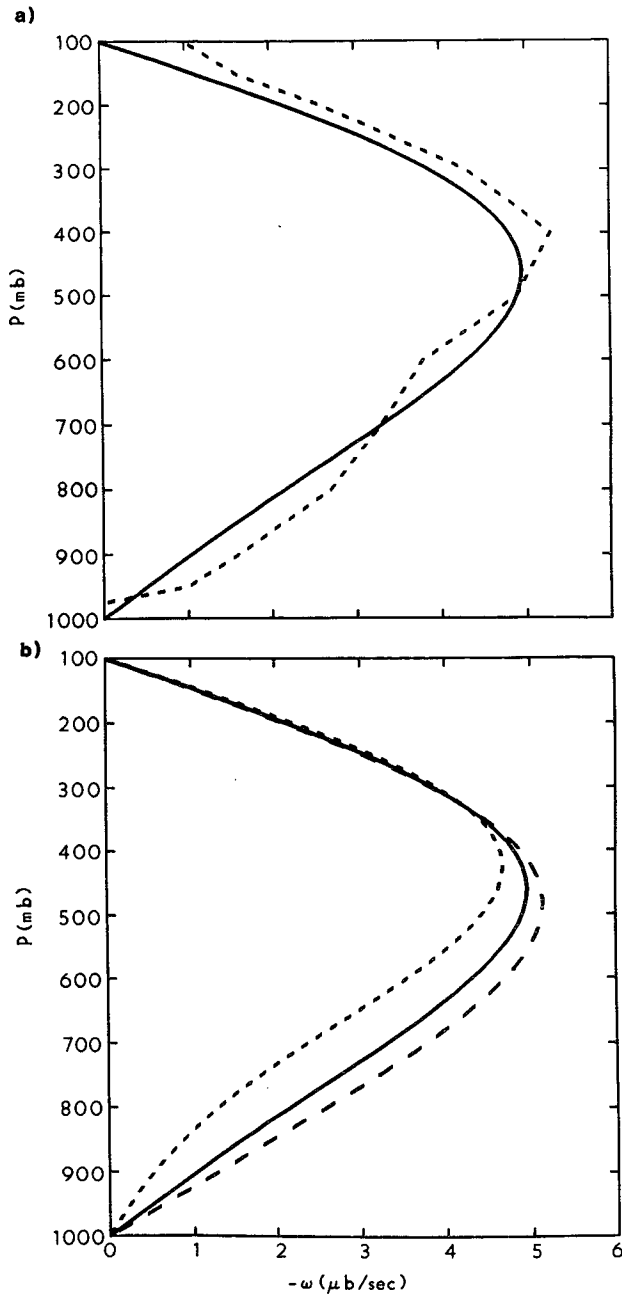


FIG. A1. (a) Vertical profile of  $\omega$ . Dashed line is calculated from observed data for a midlatitude cyclone (Palmen and Newton, 1969). Solid line is the two-mode approximation computed from (A8) and (A9). (b) Sensitivity of  $\omega$  to changes in  $F_{RHS}(700)$ . Solid line is vertical profile of  $\omega$  computed from 500- and 700-mb  $F_{RHS}$  calculated to fit the Palmen and Newton data. Long dashed line shows effect of doubling the 700-mb  $F_{RHS}$ . Short dashed line shows the effect of multiplying  $F_{RHS}$  by  $-1$ .

to approximate the data in Fig. A1 closely. Then, we examine the sensitivity of that solution to changes in the value of  $F_{RHS}$  at 700 mb.

The boundary conditions to (A6) are approximated as  $\omega = 0$  at  $p = 1000$  and 100 mb. We have data at

only two vertical levels, so the vertical variation in  $F_{RHS}$  can be resolved into just two modes. If

$$F_{RHS}(p) = a_1 \sin\left(\frac{p-100}{900}\pi\right) + a_2 \sin 2\left(\frac{p-100}{900}\pi\right), \tag{A7}$$

the solution to (A6) is

$$\omega(p) = -\left(\frac{900}{\pi f_0}\right)^2 \left[ a_1 \sin\left(\frac{p-100}{900}\pi\right) + \frac{a_2}{4} \sin 2\left(\frac{p-100}{900}\pi\right) \right]. \tag{A8}$$

A two-mode solution may be fit to the data in Fig. A1(a) by solving the following pair of linear equations for  $a_1$  and  $a_2$ :

$$\left. \begin{aligned} a_1 \sin \frac{4\pi}{9} + a_2 \left( \frac{1}{4} \sin \frac{8\pi}{9} \right) &= - \left( \frac{\pi f_0}{900} \right)^2 \omega(500) \\ a_1 \sin \frac{6\pi}{9} + a_2 \left( \frac{1}{4} \sin \frac{12\pi}{9} \right) &= - \left( \frac{\pi f_0}{900} \right)^2 \omega(700) \end{aligned} \right\}, \tag{A9}$$

where  $\omega(500)$  and  $\omega(700)$  are the 500- and 700-mb vertical velocities taken from the dashed curve in Fig. A1(a). As shown by the solid line in Fig. A1(a), this solution represents the Palmen and Newton data rather well. Having determined  $a_1$  and  $a_2$ , the values of  $F_{RHS}$  associated with the vertical velocity in Fig. A1(a) may be calculated from (A7) as:

$$\left. \begin{aligned} F_{RHS}(500) &= a_1 \sin \frac{4\pi}{9} + a_2 \sin \frac{8\pi}{9} \\ F_{RHS}(700) &= a_1 \sin \frac{6\pi}{9} + a_2 \sin \frac{12\pi}{9} \end{aligned} \right\}. \tag{A10}$$

Our first goal is now complete; values for the right-hand side forcing have been obtained which may be input to the simplified omega equation (A6) to produce a good approximation to the observed velocity profile. The 500-mb  $F_{RHS}$  is now fixed while the 700-mb  $F_{RHS}$  is perturbed. Values of  $a_1$  and  $a_2$  are obtained for the perturbed cases by solving the linear system (A10), after which the associated vertical velocity profile is obtained from (A8). The result is shown in Fig. A1(b). The solid line shows the original vertical velocity profile; the dashed lines illustrate how this changes as the 700-mb  $F_{RHS}$  is doubled (long dashes) or multiplied by  $-1$  (short dashes). The 700-mb  $\omega$  is very insensitive to the 700-mb forcing. A change in the sign of the 700-mb forcing does not change the sign of  $\omega$ .

The insensitivity of the 700-mb  $\omega$  to the 700-mb forcing is due to two factors. First the magnitude of the forcing is stronger at 500-mb than at 700-mb. Second, the longer wavelength mode is determined primarily by the 500-mb forcing, whereas the primary influence of the 700-mb forcing is on the shorter wavelength mode, and as discussed previously, the integra-

tion required to recover  $\omega$  reduces the impact of the short-wavelength forcing on the vertical velocity.

The preceding analysis is based on the assumption that the vertical-derivative term dominates the horizontal-derivative terms in the differential operator on the left-hand side of (1). In that case, the 700-mb  $\omega$  is rather insensitive to the 700-mb forcing. On the other hand, if the horizontal-derivative terms dominate, the vertical coupling will be negligible and the 700-mb  $\omega$  will depend entirely on the 700-mb forcing. If one assumes that the disturbances have a wave-like structure in all coordinate directions, the relative magnitude of the horizontal- and vertical-derivative terms depends on the ratio of the horizontal and vertical wavelengths. For typical midlatitude values of the static stability and Coriolis parameter, the horizontal- and vertical-derivative terms are of equal magnitude when the vertical scale of the disturbance is equal to the depth of the troposphere and the horizontal scale is roughly 1000 km. As the vertical scale of the disturbance decreases, or the horizontal scale increases, the vertical-derivative term begins to dominate.

Thus, in most synoptic scale situations, the coupling introduced by the vertical-derivative term is significant or dominant. As a result, the reliability of the approximation that  $\omega$  is proportional to  $-1$  times the right-hand side forcing will vary with altitude. It should work best in the midtroposphere where the forcing has a large magnitude and a strong influence on the amplitude of the dominant vertical wavelength. These results are consistent with the conclusions of TR, who found that in several case studies,  $\omega$  was best correlated with the right-hand side forcing in the midtroposphere (between 600 and 400 mb).

#### APPENDIX B

##### Finite Differencing

All the numerical computations were performed on a spherical coordinate grid with a mesh size of  $1^\circ$  latitude by  $1^\circ$  longitude. The vertical levels used in the calculations were 850, 700, 500 and 300 mb. Vertical derivatives calculated at the 500-mb level used centered differences; those calculated at the 700-mb level used data from 850 and 500 mb. Thus, the finite difference approximations to the vertical derivatives are accurate to second order in  $\Delta p$  at 500 mb, but only accurate to first order at 700 mb. However, since 700 mb is reasonably near the center of the 850 to 500 mb interval, the practical effect of this loss in accuracy should not be great. One-sided differences were used near the horizontal boundaries. The horizontal boundary points are not displayed in the figures.

Notation for the finite difference operator may be defined as

$$\delta_{nx}r(x) = (1/n\Delta x)[r(x + n\Delta x/2) - r(x - n\Delta x/2)]. \quad (\text{B1})$$

The horizontal Laplacian in spherical coordinates is computed numerically as

$$\nabla^2 r(\lambda, \phi) = \frac{1}{a^2 \cos^2 \phi} [\delta_\lambda(\delta_\lambda r) + \cos \phi \delta_\phi(\cos \phi \delta_\phi r)] \quad (\text{B2})$$

where  $a$  is the radius of the earth,  $\lambda$  is longitude and  $\phi$  is latitude (both in radians). The geostrophic wind is computed as

$$(u_g, v_g) = \frac{1}{f} \left( \frac{-1}{a} \delta_{2\phi} \Phi, \frac{1}{a \cos \phi} \delta_{2\lambda} \Phi \right). \quad (\text{B3})$$

The increase in vorticity advection with height is computed as:

$$f_0 \delta_{2p} \left[ \frac{u_g}{a \cos \phi} \delta_{2\gamma} \left( \frac{1}{f_0} \nabla^2 \Phi \right) + \frac{v_g}{a} \delta_{2\phi} \left( \frac{1}{f_0} \nabla^2 \Phi + f \right) \right]. \quad (\text{B4})$$

The Laplacian of the warm advection is computed as

$$-\nabla^2 \left[ \frac{u_g}{a \cos \phi} \delta_{2\lambda}(\delta_{2p} \Phi) + \frac{v_g}{a} \delta_{2\phi}(\delta_{2p} \Phi) \right]. \quad (\text{B5})$$

The  $Q$ -vectors,  $(q_x, q_y)$ , are computed as

$$q_x = \frac{1}{a^2 \cos^2 \phi} (\delta_{2\lambda} u_g) [\delta_{2\lambda}(\delta_{2p} \Phi)] + \frac{1}{a^2 \cos \phi} (\delta_{2\lambda} v_g) [\delta_{2\phi}(\delta_{2p} \Phi)], \quad (\text{B6})$$

$$q_y = \frac{1}{a^2 \cos^2 \phi} (\delta_{2\phi} u_g) [\delta_{2\lambda}(\delta_{2p} \Phi)] + \frac{1}{a^2} (\delta_{2\phi} v_g) [\delta_{2\phi}(\delta_{2p} \Phi)]. \quad (\text{B7})$$

Then, the forcing for  $\omega$  could be computed as

$$\frac{-2}{a \cos \phi} [\delta_{2\lambda} q_x + \delta_{2\phi}(q_y \cos \phi)]. \quad (\text{B8})$$

Equation (B8) requires the use of geopotential heights in a 24-point horizontal pattern (at three different levels) whereas the conventional forcing terms require heights in a more compact 13-point horizontal pattern. The wider numerical stencil used by (B8) tends to produce a small loss of amplitude and detail. Therefore the divergence of the  $Q$ -vectors is actually computed as follows:

$$\begin{aligned} & \frac{-2}{a \cos \phi} \left( \delta_\lambda \left\{ \frac{1}{a^2 \cos^2 \phi} (\delta_\lambda u_g) [\delta_\lambda(\delta_{2p} \Phi)] \right. \right. \\ & \quad \left. \left. + \frac{1}{a^2 \cos \phi} (\delta_\lambda v_g) [\delta_{2\phi}(\delta_{2p} \Phi^\lambda)] \right\} \right. \\ & \quad \left. + \delta_\phi \left\{ \frac{1}{a^2} (\delta_\phi u_g) [\delta_{2\lambda}(\delta_{2p} \Phi^\phi)] + \frac{\cos \phi}{a^2} (\delta_\phi v_g) [\delta_\phi(\delta_{2p} \Phi)] \right\} \right) \end{aligned} \quad (\text{B9})$$

where

$$r(x)^\lambda = (1/2)[r(x + \Delta x/2) + r(x - \Delta x/2)]. \quad (\text{B10})$$

In (B9) the  $x$ - and  $y$ -components of  $Q$  are computed at points on a staggered grid, as indicated in Fig. B1.

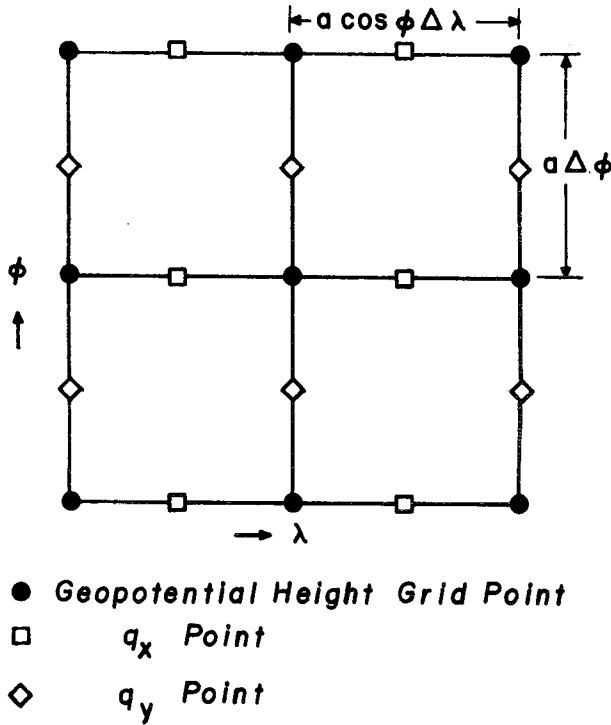


FIG. B1. The location of variables on the numerical grid.

This reduces the number of horizontal points required at each level from 24 to 13, and allows a more accurate calculation of  $\nabla \cdot \mathbf{Q}$ . However, it does not lend itself to the display of  $Q$ -vectors because the  $x$ - and  $y$ -components are not computed at the same points.

Return now to the question of why we get different results from the traditional and  $Q$ -vector forms of the omega equation. The continuous equations which represent the two forms are equivalent, but that equivalence relies on the use of the product rule, i.e.,

$$\frac{\partial AB}{\partial p} = A \frac{\partial B}{\partial p} + B \frac{\partial A}{\partial p}. \quad (\text{B11})$$

Note, however, that

$$\frac{A_{i+1}B_{i+1} - A_{i-1}B_{i-1}}{2\Delta} \neq A_i \frac{(B_{i+1} - B_{i-1})}{2\Delta} + B_i \frac{(A_{i+1} - A_{i-1})}{2\Delta}. \quad (\text{B12})$$

Thus, the numerical expression (B4) does not decompose into numerical expressions for the advection of vorticity by the thermal wind and the advection of thermal vorticity by the wind. Similarly, the numerical expression (B5) does not decompose into the terms described in (2b). Thus, the term which represents the advection of thermal vorticity by the wind does not exactly cancel when (B4) and (B5) are summed. The

residual error appears to be responsible for the differences between the traditional and  $Q$ -vector forms.

APPENDIX C

Analytic Function Used to Test Accuracy of the Finite Differences

The height field used to compare the finite difference forms of the divergence of the  $Q$ -vectors and the traditional right-hand side forcing must have continuous third derivatives along the  $x$  and  $y$  coordinates. It was specified as

$$h(x, y, 500) = 5370 + 143 \tan^{-1} \left[ \frac{\pi(y - y_c)}{2\,000\,000} \right] - 160 \left[ \left( \frac{x - x_c - x_0}{400\,000} \right)^2 + \left( \frac{y - y_c}{500\,000} \right)^2 \right]^{-1},$$

$$T(x, y, 500) = 245 + 14.3 \tan^{-1} \left[ \frac{\pi(y - y_c)}{2\,000\,000} \right] - 18 \left[ \left( \frac{x - x_c + x_0}{400\,000} \right)^2 + \left( \frac{y - y_c}{500\,000} \right)^2 \right]^{-1},$$

$$h(x, y, p) = h(x, y, 500) + 6 \left[ \left( \frac{p - 700}{200} \right)^2 - 1 \right] T(x, y, 500)$$

where  $(x_c, y_c)$  are the coordinates of the center of the domain;  $x_0 = 200$  km, one-half the distance by which the temperature trough lags the trough in the height field and  $\pi = 3.1416$ . All units are mks, with the exception of pressure which is in mb.

REFERENCES

Barnes, S. L., 1985: Omega diagnostics as a supplement to LFM/MOS guidance in weakly forced convective situations. *Mon. Wea. Rev.*, **113**, 2122-2141.  
 Haltiner, G. J., 1971: *Numerical Weather Prediction*. Wiley and Sons, 317 pp.  
 Heflick, S., and J. Fors, 1979: A simple analysis/diagnosis system for real time evaluation of vertical motion. NOAA Tech. Memo. NWS WR-138, 27 pp. [Available from National Weather Service Western Region Headquarters, Salt Lake City.]  
 Holton, J. R., 1979: *An Introduction to Dynamic Meteorology*. 2nd ed., Academic Press, 391 pp.  
 Hoskins, B. J., and M. S. Pedder, 1980: The diagnosis of middle latitude synoptic development. *Quart. J. Roy. Meteor. Soc.*, **106**, 707-719.  
 —, I. Draghici and H. C. Davies, 1978: A new look at the  $\omega$ -equation. *Quart. J. Roy. Meteor. Soc.*, **104**, 31-38.  
 Palmén, E., and C. W. Newton, 1969. *Atmosphere Circulation Systems*. Academic Press, 603 pp.  
 Pedlosky, J., 1979: *Geophysical Fluid Dynamics*. Springer-Verlag, 624 pp.  
 Saucier, W. J., 1955: *Principles of Meteorological Analysis*. University of Chicago Press, 438 pp.  
 Sutcliffe, R. C., 1947: A contribution to the problem of development. *Quart. J. Roy. Meteor. Soc.*, **73**, 370-383.  
 Trenberth, K. E., 1978: On the interpretation of the diagnostic quasi-geostrophic omega equation. *Mon. Wea. Rev.*, **106**, 131-137.